Journal of Materials Chemistry A

PAPER

View Article Online
View Journal | View Issue

Cite this: J. Mater. Chem. A, 2016, 4, 4848

Effect of particle size of $La_5Ti_2CuS_5O_7$ on photoelectrochemical properties in solar hydrogen evolution†

Jingyuan Liu,[a] Takashi Hisatomi,[a] Masao Katayama,[a] Tsutomu Minegishi,[ab] Jun Kubota‡[a] and Kazunari Domen*[a]

Received 30th December 2015
Accepted 25th February 2016

DOI: 10.1039/c5ta10731h

www.rsc.org/MaterialsA

$La_5Ti_2CuS_5O_7$ (LTC) is an oxysulphide semiconductor with spatially separated one-dimensional carrier transport properties that are applicable to sunlight-driven photoelectrochemical (PEC) water splitting. In this study, rod-like LTC particles with different sizes were prepared by controlling the annealing duration and sequential centrifugation conditions, and their PEC properties were investigated to develop a material design strategy tailored for hydrogen evolution. The larger LTC particles were found to generate a higher photocurrent. The hypothetical half-cell solar-to-hydrogen energy conversion efficiency of Mg-doped LTC reached 0.17% at 0.6 V *vs.* RHE. The faradic efficiency of the PEC hydrogen evolution was also confirmed to exceed 90%. Scanning electron microscopy images of PEC-deposited Pt nanoparticles showed that they were selectively loaded on the edge surface of large LTC particles, while they were loaded on both the lateral and edge surfaces of small LTC particles. This is presumably because the large LTC particles contained lower densities of defects and grain boundaries, interrupting the spatially separated carrier transport. Therefore, the use of well-grown, rod-like LTC particles is concluded to be favourable for PEC hydrogen production.

Introduction

Photoelectrochemical (PEC) water splitting is a promising technology for the direct conversion of solar energy into chemical energy stored in the bonds of hydrogen.[1–5] Under band-gap excitation by sunlight, hydrogen or oxygen can be produced from water on the surface of semiconductor electrodes. Many semiconductor photoelectrodes are known to generate a high photocathodic or photoanodic current under simulated sunlight and the application of a sufficiently high external voltage.[6–11] However, it currently remains difficult to drive unassisted PEC water splitting using a single photoelectrode under sunlight irradiation. One approach taken to overcome this difficulty has been the design of a p/n-PEC cell based on a series-connected photocathode and photoanode.[2,12–15] In this two-step excitation system, unassisted PEC water splitting can be achieved by matching the photocathode and photoanode photocurrents at the same electrode potential, and the reduction and oxidation of water occur separately on the surface of the respective photoelectrodes. The operating photocurrent of a p/n-PEC cell can be estimated from the intersection of steady current–potential curves of the respective photoelectrodes and is proportional to the solar-to-hydrogen energy conversion efficiency (STH).[2] Many standalone p/n-PEC cells based on this concept have been reported.[16–20]

$La_5Ti_2CuS_5O_7$ (LTC) is an oxysulphide semiconductor with an absorption edge wavelength of 650 nm that is applicable to PEC water splitting.[21–23] LTC is composed of a series of $Ti(O,S)_6$ octahedra and CuS_4 tetrahedra growing along the *b*-axis and forms rod-like particles. Density functional theory (DFT) calculations have shown that the conduction band minimum and valence band maximum of LTC are localized around linear chains of the $Ti(O,S)_6$ and CuS_4 units, respectively.[22] Therefore, photogenerated electrons and holes can move along the *b*-axis to the edge surfaces of LTC particles separately through these linear chains. The selective deposition of Pt particles on the edge surface of rod-like LTC particles by the PEC reduction of $[PtCl_6]^{2-}$ has been demonstrated.[24] The crystal structure of LTC is therefore considered to be well suited for the separation and long-range transfer of photogenerated carriers. In fact, LTC/Au electrodes fabricated by the particle transfer method have exhibited onset potentials for a photocathodic current as high as +0.8 V *vs.* RHE, which is one of the largest positive potentials

[a]Department of Chemical System Engineering, School of Engineering, The University of Tokyo, 7-3-1 Hongo, Bunkyo-ku, 113-8656 Tokyo, Japan. E-mail: domen@chemsys.t.u-tokyo.ac.jp

[b]Japan Science and Technology Agency/Precursory Research for Embryonic Science and Technology (JST/PRESTO), Kawaguchi Center Building, 4-1-8, Honcho, Kawaguchi-shi, 332-0012 Saitama, Japan

† Electronic supplementary information (ESI) available: XRD patterns, SEM images, DRS spectra, current–potential curves, time courses of PEC water splitting, and normalized IPCE spectra. See DOI: 10.1039/c5ta10731h

‡ Current address: Department of Chemical Engineering, Fukuoka University, 8-19-1 Nanakuma, Jonan-ku, 814-0180 Fukuoka, Japan.

observed among existing photocathodes,[25,26] reflecting the long lifetimes and diffusion lengths of the photogenerated carriers. Moreover, the photocurrent was increased from 0.06 to 0.2 mA cm^{-2} at 0 V *vs.* RHE under simulated AM1.5 G sunlight irradiation by doping Sc^{3+} into the Ti^{4+} sites of LTC.[27]

Although the positive onset potential of LTC for PEC hydrogen evolution is ideal for application to p/n-PEC cells with various types of photoanodes, the observed photocurrent was found to be much lower than the theoretical value of 16.8 mA cm^{-2}, which was calculated assuming an incident photon-to-current efficiency (IPCE) of unity up to the absorption edge wavelength.[3] Therefore, a material design strategy should be established to close the gap between the observed and calculated photocurrents. The morphology of LTC particles is believed to have a significant influence on the PEC performance of LTC photoelectrodes, based on the one-dimensional carrier transport properties of rod-like LTC particles. In this study, LTC particles with different sizes were prepared by controlling the annealing duration and through sequential centrifugation, and the effect of the particle size on the PEC properties was investigated.

Experimental

LTC was prepared by solid-state reactions described in the literature.[21] First, La_2O_3 (99.99%, Kanto Chemical Co., Inc.), La_2S_3 (99.9%, Kojundo Chemical Laboratory Co., Ltd.), TiO_2 (99.99%, Rare Metallic Co., Ltd.), Cu_2S (99%, Kojundo Chemical Laboratory Co., Ltd.), and sulphur (99.99%, Kojundo Chemical Laboratory Co., Ltd.) were mixed at a molar ratio of $La_2O_3 : La_2S_3 : TiO_2 : Cu_2S : S = 2 : 3 : 4 : 1 : 0.25$ in a nitrogen-circulated glovebox. The La_2O_3 and TiO_2 were respectively calcined at 1273 K for 10 h and 1073 for 1 h just prior to mixing. For the substitution of either Sc, Mg, or Al dopants into the Ti sites of LTC to enhance the photocathodic response, the amount of TiO_2 was reduced and the corresponding amount of Sc_2O_3 (99.95%, Kanto Chemical Co., Inc.), MgO (99.9%, 0.2 μm, Wako Pure Chemical Industries, Ltd), or Al_2O_3 (99.99%, 0.3 μm, Soekawa Chemicals) was added. All of the oxides were freshly calcined at 1273 K for 6 h before use. The precursor mixtures were sealed in evacuated quartz tubes and heated from room temperature to 473 K in 9 min, from 473 to 673 K in 1 h 40 min, and from 673 to 1273 K in 50 h. The temperature was then maintained at 1273 K for various durations in the range of 0–96 h. After the annealing process was complete, the samples were ground into powder. The pristine and Mg-doped LTC were suspended in 14 mL of glycerol (97%, Wako Pure Chemical Industries, Ltd) for centrifugation. Aggregated bulky particles were separated first as a sediment by centrifugation at 300 rpm for 10 min. The supernatant was collected and sequentially centrifuged at 2000, 5000, and 8000 rpm for 10 min. The powders collected from the sediments at the respective centrifugation steps were denoted as large-, medium-, and small-sized LTC particles, respectively. The samples were characterized by X-ray diffraction (XRD; RINT Ultima III, RIGAKU), UV-visible diffuse reflectance spectroscopy (UV-vis DRS; V-670, JASCO), and field-emission scanning electron microscopy (FE-SEM; S-4700, Hitachi).

LTC electrodes were fabricated using the particle transfer method.[28] LTC powder was dispersed in 2-propanol and deposited on a glass plate. After the 2-propanol evaporated, an Au layer thicker than 2 μm was deposited on the sample by vacuum evaporation. Then, carbon tape supported by a glass slide was used to peel off the composite of the Au layer and LTC powder from the original glass plate. Excess particles were removed by sonication. Subsequently, an electric wire was connected to the electrode using a solder and was covered with epoxy resin. Pt was deposited on the LTC photoelectrodes by potentiostatic photodeposition under irradiation by simulated sunlight (AM1.5 G; XES-40S2-CE, San-ei Electric Co., Ltd.) in 100 mL of a 0.1 M Na_2SO_4, 0.1 M $K_2C_2O_4$, and 3.5×10^{-6} M H_2PtCl_6 aqueous solution. A Pt wire and an Ag/AgCl electrode were used as the reference and counter electrodes, respectively. The pH of the electrolyte solution was adjusted to 10 with a 0.1 M NaOH aqueous solution. During the photodeposition reaction, the electrolyte solution was stirred under bubbling Ar.

Current–potential curves were measured with a three-electrode system using Pt and Ag/AgCl electrodes as the counter and reference electrodes, respectively. A 0.1 M Na_2SO_4 aqueous solution (100 mL) was used as the electrolyte solution, and its pH was adjusted to 10 with a 0.1 M NaOH aqueous solution. Simulated sunlight (AM1.5 G; XES-40S2-CE, San-ei Electric Co., Ltd.) was used as the light source. The potential of the LTC electrode was controlled by an automatic polarization system (HSV-100, Hokuto Denko), and the onset potential was estimated as the potential at which the photocathodic current exceeded 20 μA cm^{-2}. The variation of the photocurrent was within 15% for typical photoelectrode samples. The IPCE was measured at 0 and +0.65 V *vs.* RHE under illumination by using a 300 W Xe lamp (MAX-302, Asahi Spectra) equipped with a series of band pass filters. The photon flux of the monochromatised light was measured using a calibrated Si photodiode (Hamamatsu Photonics).

The faradic efficiency of the LTC photocathodes for PEC hydrogen evolution was measured with the same electrode system and electrolyte solution described in the above paragraph. The reactor was purged with Ar and maintained at atmospheric pressure. The LTC electrode was irradiated with visible light from a 300 W Xe lamp equipped with a cut-off filter ($\lambda > 420$ nm) and a dichroic mirror to remove UV and infrared light. The potential of the electrode was controlled as described above. The amounts of evolved hydrogen and oxygen were quantified with an on-line micro-gas chromatograph (3000A, Agilent). The faradaic efficiency was calculated as the ratio of twice the number of detected hydrogen molecules to the number of electrons observed as current.

Results and discussion

Prior to investigating the effect of the LTC particle size on its PEC properties, the PEC properties of LTC doped with 1% Sc, Mg, and Al (all calcined for 48 h) were investigated. Briefly, no significant differences in their crystallinities, particle morphologies, or light absorption properties were observed, as evaluated by XRD, SEM, and UV-vis DRS as shown in Fig. S1–S3

in the ESI,† respectively. However, the current–potential curves of the doped LTC photocathodes in aqueous solution under chopped illumination were dependent on the type of dopant, as shown in Fig. S4.† Specifically, Mg- and Al-doping increased the photocurrent of LTC more significantly than did our previously reported Sc doping,[24] and the Mg-doped LTC showed almost the same photocurrent as our recently reported Al-doped LTC.[18] Therefore, the effect of the particle size on the PEC properties of LTC was investigated in detail for Sc- and Mg-doped LTC.

Fig. 1 and 2 respectively show XRD patterns and SEM images of Sc-doped LTC maintained at 1273 K for 0–96 h. All of the samples were composed of crystalline Sc-doped LTC as the major phase and included rod-like Sc-doped LTC particles longer than 3 μm, even when the temperature was not maintained at 1273 K. This indicates that generation of the LTC phase and growth into micrometre-length particles took place during the heating from room temperature to 1273 K. The fraction of particles shorter than 1 μm in length was clearly lower for Sc-doped LTC maintained at 1273 K for 96 h than for 0 h, suggesting that the fraction of small particles can be decreased by extending the annealing duration. However, longer annealing durations did not result in an appreciable reduction in the full width at half maximum (FWHM) of the XRD peaks.

Current–potential curves of Sc-doped LTC photoelectrodes annealed for various durations in the water splitting reaction are presented in Fig. 3. The onset potential was virtually the same for all of the samples, while the photocathodic current increased with annealing duration. The Sc-doped LTC annealed for 96 h showed a 20% higher photocurrent than our previously reported sample annealed for 48 h at 0 V *vs.* RHE.[24] Mg-doped LTC also followed the same trend with regard to annealing duration. Specifically, the photocathodic current increased with increasing annealing duration and reached 0.5 mA cm^{-2} at 0 V *vs.* RHE at an annealing duration of 96 h (Fig. S5†), which was approximately 30% higher than that observed for the Sc-doped LTC photocathode. These results suggest that larger LTC particles exhibit higher photocurrents. By using photoelectrodes made from the Mg-doped LTC particles heated for 96 h, the hypothetical half-cell solar-to-hydrogen (HC-STH) energy conversion efficiency[5] reached 0.17% at 0.6 V *vs.* RHE (Fig. 4). The faradic efficiency for PEC hydrogen evolution was estimated to be 93% at both 0 and 0.65 V *vs.* RHE (Fig. S6†). The peaking of the HC-STH energy conversion efficiency at 0.6 V *vs.* RHE and the faradic efficiency of almost unity at a positive potential indicate that Mg-doped LTC is a promising photocathode for application in p/n-PEC cells.

The length of the LTC particles in the longitudinal direction varied widely from ~0.1 to ~10 μm. To discuss the effect of the particle size on the PEC properties of LTC electrodes more rigorously, particle size classification was carried out by sequential centrifugation. The effect of centrifugation on the particle size classification was essentially identical regardless of

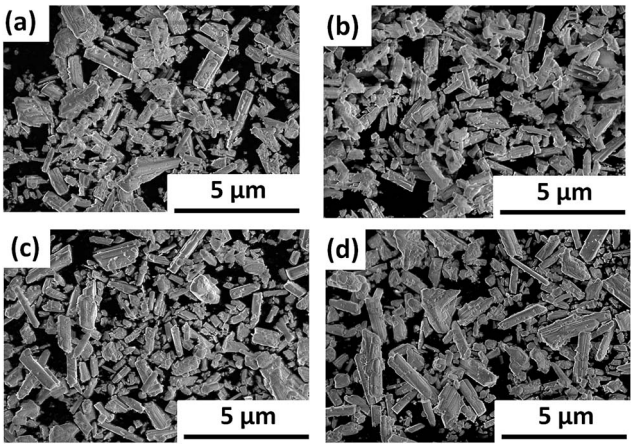

Fig. 2 SEM images of Sc-doped LTC powders synthesized with annealing durations of (a) 0, (b) 5, (c) 48, and (d) 96 h.

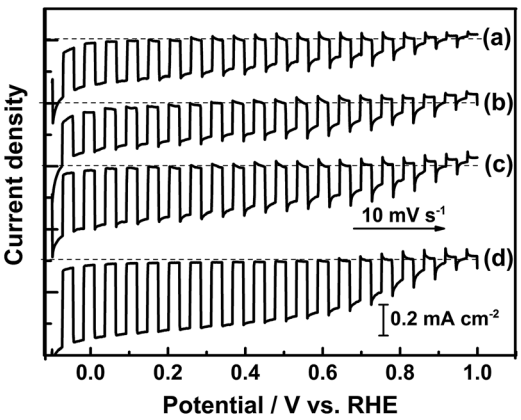

Fig. 3 Current–potential curves of photocathodes of Sc-doped LTC powders synthesized with annealing durations of (a) 0, (b) 5, (c) 48, and (d) 96 h. The measurements were carried out in a 0.1 M Na_2SO_4 aqueous solution (pH 10) under chopped simulated sunlight irradiation. The photocathodes were modified with Pt by photodeposition.

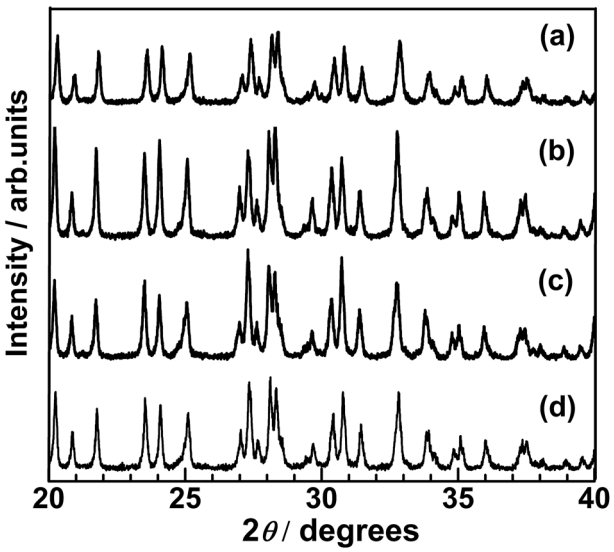

Fig. 1 XRD patterns of Sc-doped LTC powders synthesized with annealing durations of (a) 0, (b) 5, (c) 48, and (d) 96 h.

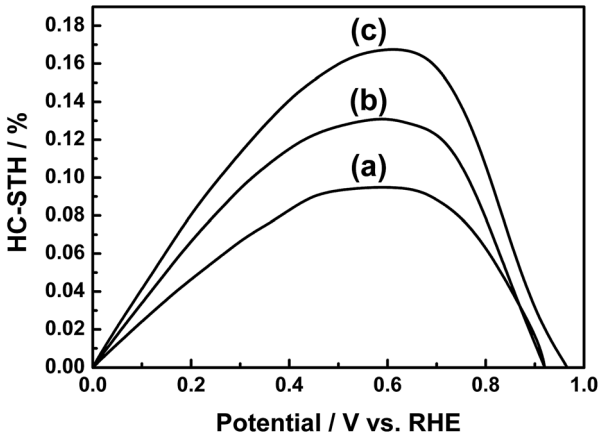

Fig. 4 HC-STH for PEC hydrogen evolution using photocathodes of (a) Sc-doped LTC annealed for 48 h, (b) Sc-doped LTC annealed for 96 h, and (c) Mg-doped LTC annealed for 96 h.

the dopant. Fig. 5 shows SEM images of LTC particles annealed at 1273 K for 48 h before and after sequential centrifugation. After the sequential centrifugation, LTC particles were size-classified roughly into lengths of <2, 2–4, and >4 μm, which accounted for 10%, 30%, and 30% of the sample by weight, and these groups were designated as small-, medium-, and large-sized LTC, respectively. The remaining 30% of the sample was composed of aggregates of LTC particles without clear columnar shapes, and is excluded from the following discussion.

XRD patterns of the size-classified LTC samples are presented in Fig. 6. The LTC samples exhibited the exact diffraction patterns expected for the LTC phase. The FWHM of the diffraction peaks did not consistently depend on the particle size; specifically, some diffraction peaks were narrower for the large-sized LTC while others were narrower for the medium-sized LTC. This is likely because the large-sized and medium-sized LTC consisted of well-crystalline anisotropic micrometre-size particles. In fact, the relative intensities of the XRD peaks for the samples, particularly for the large-sized LTC, deviated

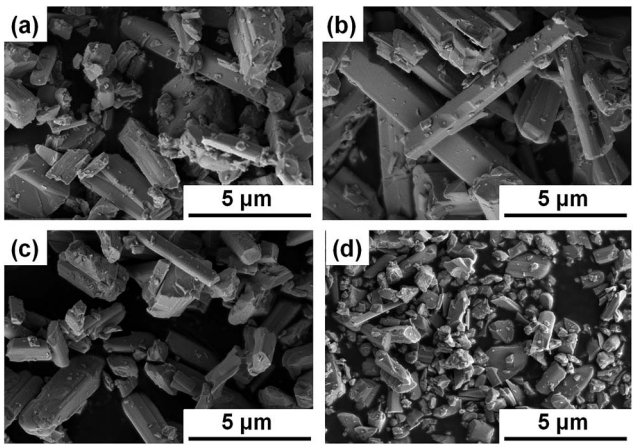

Fig. 5 SEM images of (a) pristine, (b) large-, (c) medium-, and (d) small-sized undoped LTC particles.

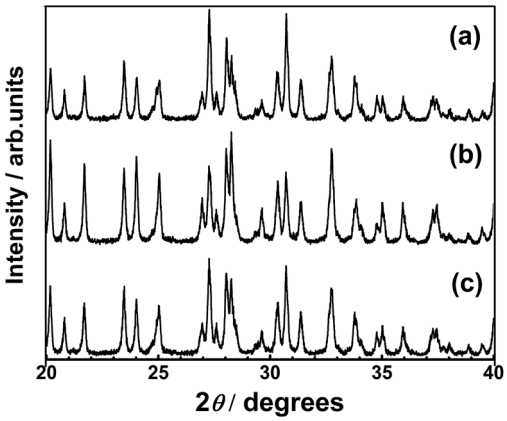

Fig. 6 XRD patterns of (a) pristine, (b) large- and (c) medium-sized undoped LTC.

from those simulated from the literature data.[21] In addition, most of the isolated peaks in Fig. 6 originated from (*k*0*l*) diffractions. For these reasons, the FWHM may not reflect the longitudinal lengths of the rod-like LTC particles.

Current–potential curves of the size-classified Mg-doped LTC electrodes for the water splitting reaction are presented in Fig. 7. Here, Mg-doped LTC annealed for 48 h was employed as a pristine sample because it generated a higher photocurrent than the undoped and Sc-doped LTC powders, and therefore the effect of the particle size on the PEC properties would be observed more clearly. The onset potential of the photocathodic current did not vary significantly; however, the photocurrent clearly increased with increasing average particle size, although all of the samples had the same thermal history. This observation agrees well with the results observed for doped LTC powders prepared with different annealing durations. Based on these results, it is concluded that larger LTC particles exhibit higher photocurrent for the PEC water splitting reaction.

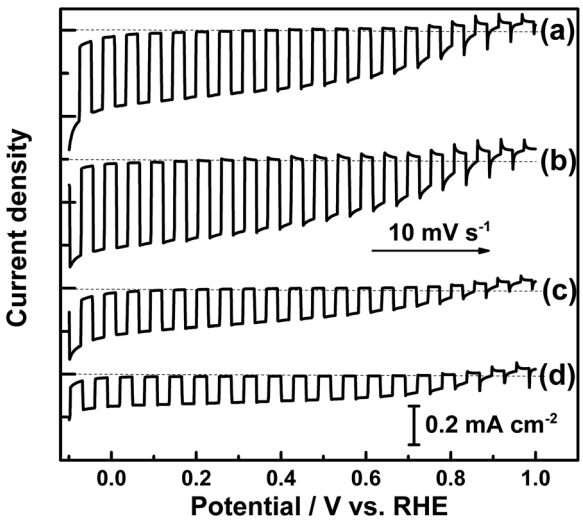

Fig. 7 Current–potential curves of (a) pristine, (b) large-, (c) medium- and (d) small-sized Mg-doped LTC photocathodes under chopped illumination.

The magnitude of the photocathodic current corresponds to the number of electrons that survive recombination and contributes to water reduction on the LTC surface. The behaviour of photoexcited carriers in a given photoelectrode can be controlled *via* the electrode potential and the incident photon wavelength, because these determine the width of the space charge layer and the penetration depth of incident photons, respectively. Therefore, the similarities and differences in the PEC properties of LTC particles with different sizes can be clarified through an investigation of the IPCE at different electrode potentials. Fig. 8 shows the IPCE spectra of electrodes composed of Mg-doped LTC particles of different sizes. The IPCE increased at shorter wavelengths and more negative potentials regardless of the particle size. This is because more photons are absorbed near the surface due to the increase in the absorption coefficient, and because the recombination of surface-trapped minority carriers with majority carriers in the bulk of Mg-doped LTC particles is suppressed at more negative potentials owing to the enhanced band bending. The IPCE of the electrode made from large-sized Mg-doped LTC particles was 2.2% at 420 nm and at 0 V *vs.* RHE, which is 3.6 times higher than the value of 0.6% observed for the small-particle sample. Notably, the IPCE profiles of Mg-doped LTC photocathodes virtually overlapped upon normalization regardless of the particle sizes and the electrode potentials (Fig. S7†). In general, the width of the space charge layer of a semiconductor electrode is proportional to the square root of the potential difference from the flat-band potential for a given electrode specimen. Therefore, a smaller fraction of photons should be absorbed within the space charge layer for a photoelectrode composed of large LTC particles held at a positive potential. Our experimental results suggest that the behaviour of photoexcited carriers was rather insensitive to whether photons were absorbed within the space charge layer or not. This differs from the case of hematite photoanodes, which are characterized by minority carriers with an extremely short diffusion length. Here, the onset of and the increase in the IPCE occur at shorter wavelengths with smaller applied voltages for hematite photoanodes.[29–32] There are two possible reasons for this difference: (i) photons absorbed outside of the space charge layer of Mg-doped LTC can contribute to the photocurrent or (ii) the space charge layer covers the entirety of the Mg-doped LTC particles, so that all of the photons are absorbed within the space charge layer. We believe that the former is more feasible because the diffusion length of photoexcited carriers in LTC was recently suggested to be on the order of micrometres based on transient absorption spectroscopy and a numerical analysis.[33] Moreover, the latter case is unlikely for semiconducting particles of several micrometres in length held at a moderately positive potential of +0.65 V *vs.* RHE. One may think that the use of larger Mg-doped LTC particles is more favourable simply because they can absorb more photons than smaller particles. However, it is suggested by our preliminary DRS analysis that the absorptance of LTC particle layers differed only 10% for electrodes made of large-sized and small-sized LTC particles. Accordingly, a comparison of the IPCE profiles at different electrode potentials and the absorptance did not clarify the dependence of the PEC properties of the LTC photocathodes on the particle size.

The surfaces of the photoelectrodes made from the Mg-doped LTC of different particle sizes were analysed by SEM. As shown in Fig. 9, Pt nanoparticles were deposited only on the edge surfaces of the large-sized Mg-doped LTC particles, similar to the Sc-doped LTC of our previous study.[23] However, we found that Pt nanoparticles were deposited on the lateral surface as well as on the edge surfaces of the small- and medium-sized Mg-doped LTC particles. It appears that electrons migrated not only through the conduction band minimum localized around the

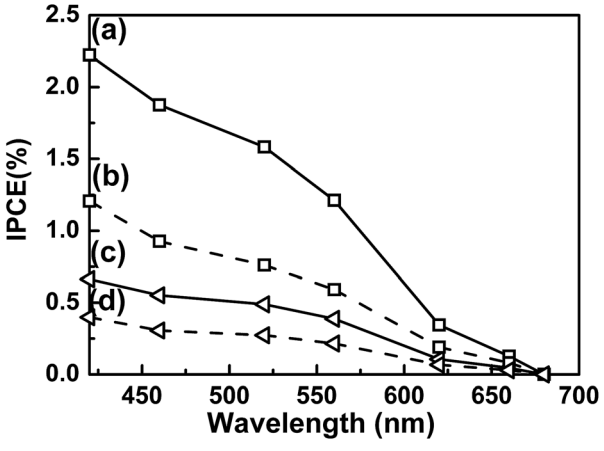

Fig. 8 IPCE spectra of (a and b) large-sized Mg-doped LTC measured at (a) 0 and (b) 0.65 V *vs.* RHE and (c and d) small-sized Mg-doped LTC measured at (c) 0 and (d) 0.65 V *vs.* RHE in Na_2SO_4 aqueous solution adjusted to pH 10. The photocathodes were modified with Pt by photodeposition.

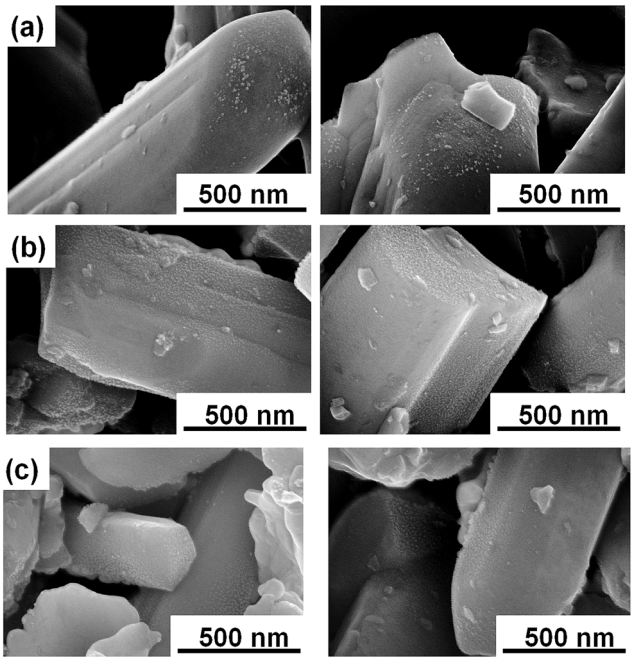

Fig. 9 Top-view SEM images of electrodes of (a) large-sized, (b) medium-sized, and (c) small-sized Mg doped-LTC after PEC measurements.

$Ti(O,S)_6$ linear chains but also through mid-gap states presumably originating from defects and grain boundaries, and emerged from the lateral face. Carrier transfer through mid-gap states would enhance the recombination of electrons and holes because the transfer paths for electrons and holes are not spatially separated. Although no significant difference was observed in the crystallinity and IPCE profiles of the different size-classified LTC particles, the inhibition of electron conduction through mid-gap states is likely a factor that enhanced the PEC properties of the large-sized LTC particles. We believe that the use of well-grown, rod-like LTC particles is preferable for PEC water splitting, at least up to lengths in the order of micrometres, because the diffusion lengths of the carriers in LTC are estimated to be of the same order.[33]

Conclusions

Size-classified, rod-like LTC particles were obtained by controlling the annealing duration and centrifugation rate. Rod-like LTC particles with larger sizes were found to exhibit higher photocurrents. The IPCE profiles of the LTC particles were nearly identical regardless of the particle sizes and the electrode potentials. However, SEM observations revealed that Pt nanoparticles were PEC-deposited not only on the edge surfaces but also on the lateral surface of small Mg-doped LTC particles, while they were selectively deposited on the edge surfaces of large Mg-doped LTC particles. This suggests that electron conduction occurred in part *via* mid-gap states and enhanced charge recombination of photoelectrodes composed of small LTC particles. Based on the results of this study, we conclude that the use of well-grown, rod-like LTC particles is advantageous for PEC hydrogen production. The peaking of the HC-STH at +0.6 V *vs.* RHE and the almost unity faradic efficiency at a positive potential render doped-LTC photoelectrodes suitable for the construction of p/n PEC cells.

Acknowledgements

This work was financially supported by Grants-in-Aids for Specially Promoted Research (No. 23000009), Young Scientists (A) (No. 15H05494), and Young Scientists (B) (No. 5K17895), and by the A3 Foresight Program of the Japan Society for the Promotion of Science (JSPS). One of the authors (J. L.) gratefully acknowledges the support of a Japan Chemical Industry Association (JCIA) Fellowship. This work was partly supported by the Artificial Photosynthesis Project of the New Energy and Industrial Technology Development Organization (NEDO).

Notes and references

1 M. Gratzel, *Nature*, 2001, **414**, 338.
2 M. G. Walter, E. L. Warren, J. R. McKone, S. W. Boettcher, Q. Mi, E. A. Santori and N. S. Lewis, *Chem. Rev.*, 2010, **110**, 6446.
3 Z. Chen, T. F. Jaramillo, T. G. Deutsch, A. Kleiman-Shwarsctein, A. J. Forman, N. Gaillard, R. Garland, K. Takanabe, C. Heske, M. Sunkara, E. W. McFarland, K. Domen, E. L. Miller, J. A. Turner and H. N. Dinh, *J. Mater. Res.*, 2010, **25**, 3.
4 F. E. Osterloh, *Chem. Soc. Rev.*, 2013, **42**, 2294.
5 T. Hisatomi, J. Kubota and K. Domen, *Chem. Soc. Rev.*, 2014, **43**, 7520.
6 M. Moriya, T. Minegishi, H. Kumagai, M. Katayama, J. Kubota and K. Domen, *J. Am. Chem. Soc.*, 2013, **135**, 3733.
7 H. Wang, T. Deutsch and J. Turner, *J. Electrochem. Soc.*, 2008, **155**, 91.
8 A. Paracchino, V. Laporte, K. Sivula, M. Grätzel and E. Thimsen, *Nat. Mater.*, 2011, **10**, 456.
9 Y. Li, L. Zhang, A. Torres-Pardo, J. M. Gonzalez-Calbet, Y. Ma, P. Oleynikov, O. Terasaki, S. Asahina, M. Shima, D. Cha, L. Zhao, K. Takanabe, J. Kubota and K. Domen, *Nat. Commun.*, 2013, **4**, 2566.
10 I. Cesar, A. Kay, J. Martinez and M. Grätzel, *J. Am. Chem. Soc.*, 2006, **128**, 4582.
11 Y. Liang, T. Tsubota, L. Mooij and R. Krol, *J. Phys. Chem. C*, 2011, **115**, 17594.
12 A. Nozik, *Appl. Phys. Lett.*, 1976, **29**, 150.
13 E. Selli, G. Chiarello, E. Quartarone, P. Mustarelli, I. Rossetti and L. Forni, *Chem. Commun.*, 2007, 5022.
14 Y. Pihosh, I. Turkevych, K. Mawatari, J. Uemura, Y. Kazoe, S. Kosar, K. Makita, T. Sugaya, T. Matsui, D. Fujita, M. Tosa, M. Kondo and T. Kitamor, *Sci. Rep.*, 2015, **5**, 11141.
15 A. Nozik, *Appl. Phys. Lett.*, 1977, **30**, 567.
16 M. G. Kibria, F. A. Chowdhury, S. Zhao, B. AlOtaibi, M. L. Trudeau, H. Guo and Z. Mi, *Nat. Commun.*, 2015, **6**, 6797.
17 M. Prevot and K. Sivula, *J. Phys. Chem. C*, 2013, **117**, 17879.
18 T. Hisatomi, S. Okamura, J. Liu, Y. Shinohara, K. Ueda, T. Higashi, M. Katayama, T. Minegishi and K. Domen, *Energy Environ. Sci.*, 2015, **8**, 3354.
19 F. Abdi, L. Han, A. Smets, M. Zeman, B. Dam and R. Krol, *Nat. Commun.*, 2013, **4**, 2195.
20 F. Jiang, Gunawan, T. Harada, Y. Kuang, T. Minegishi, K. Domen and S. Ikeda, *J. Am. Chem. Soc.*, 2015, **137**, 13691.
21 V. Meignen, L. Cario, A. Lafond, Y. Moëlo, C. Guillot-Deudon and A. Meerschaut, *J. Solid State Chem.*, 2004, **177**, 2810.
22 T. Suzuki, T. Hisatomi, K. Teramura, Y. Shimodaira, H. Kobayashi and K. Domen, *Phys. Chem. Chem. Phys.*, 2012, **14**, 15475.
23 M. Katayama, D. Yokoyama, Y. Maeda, Y. Ozaki, M. Tabata, Y. Matsumoto, A. Ishikawa, J. Kubota and K. Domen, *Mater. Sci. Eng., B*, 2010, **173**, 275.
24 G. Ma, J. Liu, T. Hisatomi, T. Minegishi, Y. Moriya, M. Iwase, H. Nishiyama, M. Katayama, T. Yamada and K. Domen, *Chem. Commun.*, 2015, **51**, 4302.
25 R. C. Valderrama, P. J. Sebastian, J. Pantoja Enriquez and S. A. Gamboa, *Sol. Energy Mater. Sol. Cells*, 2005, **88**, 145.
26 H. Wang and J. A. Turner, *J. Electrochem. Soc.*, 2010, **157**, 173.
27 J. Liu, T. Hisatomi, G. Ma, A. Iwanaga, T. Minegishi, Y. Moriya, M. Katayama, J. Kubota and K. Domen, *Energy Environ. Sci.*, 2014, **7**, 2239.
28 T. Minegishi, N. Nishimura, J. Kubota and K. Domen, *Chem. Sci.*, 2013, **4**, 1120.

29 M. Dare-Edwards, J. Goodnough, A. Hamnett and P. Trevellick, *J. Chem. Soc., Faraday Trans.*, 1983, **79**, 2027.
30 J. Kennedy and K. Frese, *J. Electrochem. Soc.*, 1978, **125**, 709.
31 T. Hisatomi, H. Dotan, M. Stefik, K. Sivula, A. Rothschild, M. Grätzel and N. Mathews, *Adv. Mater.*, 2012, **24**, 2699.
32 A. Kay, I. Cesar and M. Grätzel, *J. Am. Chem. Soc.*, 2006, **128**, 15714.
33 G. Ma, Y. Suzuki, R. Singh, A. Iwanaga, Y. Moriya, T. Minegishi, J. Liu, T. Hisatomi, H. Nishiyama, M. Katayama, K. Seki, A. Furube, T. Yamadabd and K. Domen, *Chem. Sci.*, 2015, **6**, 4513.